

The Contribution of the Intergalactic Medium to Cosmic Microwave Background Anisotropies.

F. Atrio-Barandela

*Física Teórica, Universidad de Salamanca.
Plaza de la Merced s/n. 37008 Salamanca, Spain*

atrio@usal.es

and

J.P. Mücke

*Astrophysikalisches Institut Potsdam.
D-14482 Potsdam, Germany.*

jpmuecket@aip.de

ABSTRACT

We compute the power spectrum of the Cosmic Microwave Background temperature anisotropies generated by the Intergalactic Medium. To estimate the electron pressure along the line of sight and its contribution to the Sunyaev-Zeldovich component of the CMB anisotropies, we assume the non-linear baryonic density contrast is well described by a log-normal distribution. For model parameters in agreement with observations and for an experiment operating in the Rayleigh-Jeans regime, the largest IGM contribution corresponds to scales $l \approx 2000$. The amplitude is rather uncertain and could be as large as $100 - 200 \mu\text{K}^2$, comparable to the contribution of galaxy clusters. The actual value is strongly dependent on the gas polytropic index γ , the amplitude of the matter power spectrum σ_8 , namely $C_l^{IGM} \sim (\gamma^2 \sigma_8)^{12}$. At all redshifts, the largest contribution comes from scales very close to the baryon Jeans length. This scale is not resolved in numerical simulations that follow the evolution of gas on cosmological scales. The anisotropy generated by the Intergalactic Medium could make compatible the excess of power measured by Cosmic Background Imager (CBI) on scales of $l \geq 2000$ with $\sigma_8 = 0.9$. Taking the CBI result as an upper limit, the polytropic index can be constraint to $\gamma < 1.5$ at 2σ level at redshifts $z \sim 0.1 - 0.4$. With its large frequency coverage, the PLANCK satellite will be able to measure the secondary anisotropies coming from hot gas. Cluster

and Intergalactic Medium contributions could be separated by cross correlating galaxy/cluster catalogs with CMB maps. This measurement will determine the state of the gas at low and intermediate redshifts.

Subject headings: Cosmic Microwave Background. Cosmology: theory. Cosmology: observations.

1. Introduction

In the last decade, numerical simulations (Cen & Ostriker 1999; Dave et al. 1999, 2001) and observational evidence (Rauch 1998; Stocke, Shull & Penton 2004) indicate that the highly ionized intergalactic gas has evolved from the initial density perturbations into a complex network of mildly non-linear structures in the redshift interval $0 < z < 6$, called cosmic web. This structure could contain most of the baryons in the Universe (Rauch et al. 1997; Schaye 2001; Fukugita & Peebles, 2004). With cosmic evolution, the fraction of baryons in these structures decreases as more matter is concentrated within compact virialized objects. The Ly α forest absorbers at low redshifts are filaments (with low HI column densities) containing about 30% of all baryons (Stocke et al. 2004). Hydrodynamical simulations predict that another large fraction of all baryons resides within mildly-nonlinear structures which are partly shock-confined gas filaments heated up to temperatures of $10^5 - 10^7 K$, called Warm-Hot Intergalactic Medium (WHIM). The amount of baryons within this WHIM is estimated to reach 20 - 40 % (Cen & Ostriker 1999; Dave et al. 1999, 2001).

In this article we compute the electron pressure along the line of sight of both the ionized gas in the Ly α forest and the hot gas in the WHIM. Even if the temperature of the gas in these absorbing filaments is relatively low (usually less than $10^5 K$) the total amount of ionized gas is large. This electron pressure induces distortions and temperature anisotropies on the Cosmic Microwave Background (CMB) spectrum by the Thermal Sunyaev-Zeldovich (TSZ) effect (Sunyaev & Zeldovich, 1972, 1980) as do clusters of galaxies. Early calculations of the TSZ power spectrum used analytical approaches (Atrio-Barandela & Mücke 1999; Komatsu & Kitayama 1999, Hernández-Monteagudo, Atrio-Barandela & Mücke 2000; Molnar & Birkinshaw 2000). Numerical simulations were soon used to make more accurate predictions (Refregier et al. 2000, Refregier & Teyssier 2002, Zhang, Peng & Wang 2002). Da Silva et al. (2001) studied the relative contribution from high and low density gas and found that in all models considered, the high density gas in halos dominated the TSZ signal. White et al. (2002) noticed that at $l = 2000$ about 25% of the signal came from gas in regions with density smaller than one hundred times the cosmological mean. At $l = 6000$ the contribution from the diffuse gas was less than 2%.

Numerical simulations currently agree with the predictions based on the halo model and it is reasonable to expect that the physics of baryons on dense environments has been well described in cosmological simulations. What has not been proven is whether numerical simulations have reached convergence, i.e, if further increments in resolution will not increase the signal (Bond et al. 2005). To study numerically the evolution of the complex network of filaments that develops when the evolution of the gas in low density regions becomes non-linear, requires computer resources that are at present unavailable. Soft Particle Hydrodynamics (SPH) codes do not have enough resolution and Adaptive Refinement Methods (ARM) are controlled by density and follow the evolution of high dense regions. To study the low dense regions with similar accuracy is computationally very expensive.

In this article we study the contribution coming from baryons located in the low dense regions that constitute the IGM. The web of cosmic filaments corresponds to scales in between large scale fluctuations and strongly nonlinear scales inside halos. The halo model is likely to fail to account for its complicated geometry and an analytical treatment would require a different approach. We shall use a log-normal probability distribution function (PDF) to describe the non-linear evolution of baryons in low density environments. Briefly, in Sec 2 we describe the model and in Sec 3 we derive the expressions that give the contribution of the IGM to the average y -parameter and CMB temperature anisotropies. In Sec. 4 we discuss our results and their dependence with cosmological and physical parameters. In Sec. 5 we present our conclusions and the observational prospects to measure the anisotropies generated by the IGM.

2. The Log-normal Baryon Distribution Model.

Inverse Compton scattering of CMB photons by hot gas along the line of sight produces both temperature anisotropies and distortion of the CMB spectrum. We shall assume that baryons are distributed like a lognormal random field. The log-normal distribution was introduced by Coles and Jones (1991) as a model for the non-linear distribution of matter in the Universe. Bi & Davidsen (1997) have used it as a model to describe the Ly α forest and found it reproduced the observations well. Choudhury, Padmanabhan & Srianand (2001) have introduced an analytical formalism that correctly describes the clustering properties of the neutral hydrogen in the mildly non-linear regime. We shall follow their approach to describe the distribution not of the neutral gas but of the highly ionized phase of the IGM.

If the distribution of baryons is given by a log-normal random field then the probability $P(\xi)$ that at any spatial position \mathbf{x} at redshift z the baryon (non-linear) density contrast has

the value $\xi = n_B(\mathbf{x}, z)/n_0(z)$ is given by

$$P(\xi) = \frac{1}{\xi \sqrt{2\pi} \Delta_B} e^{-\frac{(\log(\xi) + \Delta_B^2/2)^2}{2\Delta_B^2}}. \quad (1)$$

Hereafter we shall represent the linear density contrast by δ and the non-linear log-normal random field by ξ . The baryon number density $n_B(\mathbf{x}, z)$ is given by

$$n_B(\mathbf{x}, z) = n_0(z) e^{\delta_B(\mathbf{x}, z) - \Delta_B^2(z)/2}, \quad (2)$$

where \mathbf{x} denotes the spatial position at redshift z and $|\mathbf{x}(z)|$ is the proper distance; $\delta_B(\mathbf{x}, z)$ is the baryon (linear) density contrast, $n_0(z) = \rho_B(1+z)^3/\mu_B m_p$ and ρ_B, m_p are the baryon density and proton mass, respectively. The linear baryon power spectrum is related to the DM power spectrum by (Fang et al. 1993)

$$P_B^{(3)}(k, z) = \frac{P_{\text{DM}}^{(3)}(k, z)}{(1 + x_b^2(z)k^2)^2}, \quad (3)$$

where

$$x_b(z) = \frac{1}{H_0} \left[\frac{2\gamma k_B T_m(z)}{3\mu m_p \Omega_m (1+z)} \right]^{1/2}, \quad (4)$$

is the comoving Jeans length, T_m is the averaged temperature of the IGM, γ is the polytropic index, Ω_m is the cosmological fraction of matter density, $\mu = 4/(8-5Y)$ is the mean molecular weight of the IGM and $Y = 0.24$ is the helium weight fraction. The Jeans length defines the scale below which baryon perturbations are suppressed with respect to those of the DM. Only scales larger are allowed to grow. We use the log-normal statistics to describe the non-linear evolution of those perturbations at any given epoch z . Finally,

$$\Delta_B^2(z) = \langle \delta_B^2(\mathbf{x}, z) \rangle = D^2(z) \int \frac{d^3k}{(2\pi)^3} \frac{P_{DM}(k)}{[1 + x_b^2(z)k^2]^2}, \quad (5)$$

where $D(z) = D(z, \Omega_\Lambda, \Omega_m)$ is the linear growth factor.

At each redshift, the fraction $\eta(\xi_{max})$ of matter in regions with over-densities smaller or equal than a fixed value ξ_{max} is

$$\eta(\xi_{max}) = 1 - \int_{\xi_{max}}^{\infty} P(\xi) d\xi \quad (6)$$

At each redshift, the fraction of matter in regions with over-density larger than a fixed value ξ_{max} is $1 - \eta(\xi_{max})$. In Fig. 1 we plot the fraction of matter that resides in regions with over-density $\xi \geq 10, 50, 100$ and 500 at different redshifts. Since the log-normal PDF is rather skewed, the fraction of matter in high dense regions is not negligible. As the figure

indicates, when the expansion of the Universe starts to accelerate (around $z = 0.5$) this fraction becomes constant. Below this redshift, the fraction of matter with density contrasts $\xi > 100$ is less than 0.3%.

The number density of electrons n_e in the IGM can be obtained by assuming ionization equilibrium between recombination and photo-ionization and collisional ionization. At the conditions valid for the IGM (temperature in the range $10^4 - 10^7$ K, and density contrast $\xi < 100$) the degree of ionization is very high. Commonly $n_e = \epsilon n_B$, with $0.9 < \epsilon \leq 1$ depending on the degree of ionization. To compute the temperature of the IGM at each position and redshift we use a polytropic equation of state

$$T(\mathbf{x}, z) = T_0(z) \left(\frac{n_B(\mathbf{x}, z)}{n_0(z)} \right)^{\gamma-1}, \quad (7)$$

where T_0 is the temperature of the IGM at mean density n_0 at given redshift z .

3. Comptonization Parameter and Radiation Power Spectrum.

The contribution to the Comptonization parameter of a patch of hot gas of size L at a proper distance $l = |\mathbf{x}|$ is (Sunyaev & Zel'dovich 1972)

$$\Delta y_c(z, \mathbf{x}) = y_0 \int_0^L T_e(\mathbf{x}, z) n_e(\mathbf{x}, z) dl, \quad (8)$$

where $y_0 = k_B \sigma_T / m_e c^2 g(\nu)$. Constants have their usual meaning and $g(\nu)$ is the frequency dependence of the SZ effect. The average line of sight contribution coming from structures located at z is

$$\Delta y_c(z) = y_0 \int_0^L \langle n_e(\mathbf{x}, z) T_e(\mathbf{x}, z) \rangle dl. \quad (9)$$

The average is carried out over the whole spatial volume at redshift z . The total contribution up to redshift z_f at which the Universe is fully re-ionized is

$$y_{c,av} = y_0 \int_0^{z_f} \langle n_e(\mathbf{x}, z) T_e(\mathbf{x}, z) \rangle \frac{dl}{dz} dz. \quad (10)$$

Substituting the expressions of n_e and T obtained assuming a lognormal gas distribution gives

$$y_{c,av} = y_0 \int_0^{z_f} n_0(z) T_0(z) e^{[(\gamma^2 - \gamma)\Delta^2(z)/2]} \frac{dl}{dz} dz. \quad (11)$$

Numerically, we shall restrict the average on eq. (9) to baryons residing in over-densities $\xi \leq \xi_{max}$ (which for concreteness we shall take equal to 100) to exclude those baryons that

could not be correctly described by the log-normal model (see below). Therefore, at each redshift we compute

$$\langle f(\xi) \rangle_{|\xi_{max}} = \int^{\xi_{max}} f(\xi) P(\xi) d\xi \quad (12)$$

The power spectrum contribution of the CMB temperature anisotropies induced by the IGM can be obtained from the 2-point correlation function of the spatial variations of the electron pressure:

$$C(\theta) = \int_0^{z_f} \int_0^{z_f} \Delta y_c(z) B(\theta, z, z') \Delta y_c(z') \frac{dl}{dz} \frac{dl'}{dz'} dz dz'. \quad (13)$$

In this expression $\Delta y_c(z)$ is given by eq. (9), $B(\theta, z, z') = e^{[\gamma^2 Q(|\mathbf{x} - \mathbf{x}'|, z, z')]} - 1$ is the normalized two-point correlation function with

$$Q(|\mathbf{x} - \mathbf{x}'|, z, z') = \frac{D(z, \Omega_\Lambda, \Omega_m) D(z', \Omega_\Lambda, \Omega_m)}{2\pi^2} \int_0^\infty \frac{P_{DM}(k) k^2}{[1 + x_b^2(z) k^2][1 + x_b^2(z') k^2]} \frac{\sin(k|\mathbf{x} - \mathbf{x}'|)}{k|\mathbf{x} - \mathbf{x}'|} dk. \quad (14)$$

In here $|\mathbf{x} - \mathbf{x}'|$ denotes the proper distance between two patches at positions $\mathbf{x}(z)$ and $\mathbf{x}'(z')$ separated by the angle θ . In the flat sky approximation

$$|\mathbf{x} - \mathbf{x}'| \approx \sqrt{l_\perp(\theta, z)^2 + [r(z) - r(z')]^2}, \quad (15)$$

where $l_\perp(\theta, z)$ is the transversal distance of two points located at the same redshift. Within this approximation, the correlation function is dominated by patches that are physically very close. For small θ , the correlation between patches at different redshifts is negligible and $B(\theta, z, z') \simeq B(\theta, z, z) \delta_{Dirac}(z - z')$ is accurate at the 1% level. Eq. (13) can be simplified to give

$$C(\theta) = y_0^2 \int_0^{z_l} \left[\frac{dl}{dz} \right]^2 n_0^2(z) T_0^2(z) e^{\gamma(\gamma-1)\Delta^2(z)} [e^{\gamma^2 Q(\theta, z)} - 1] dz \quad (16)$$

This approximation to the eq. (13) fails at large angular scales but, since at those scales the correlation is negligible, it does not affect the numerical results while greatly speeds up the computer code. Like for the Comptonization parameter $y_{c,av}$, we restrict the average to baryons within the mildly-nonlinear regime, i.e., $\xi \leq \xi_{max} = 100$. Finally, the power spectrum can be obtained by Fourier transform:

$$C_l^{IGM} = 2\pi \int_{-1}^{+1} C(\theta) P_l(\cos \theta) d(\cos \theta), \quad (17)$$

where P_l denotes the Legendre polynomial of multipole l .

Since $y_{c,av}$ and C_l^{IGM} depend on the electron pressure and not separately on the IGM temperature or density, eqs. (11) and (16) scale with IGM mean temperature T_0 and ionization fraction ϵ as $(T_0 \epsilon)$ to some power. The uncertainty in the degree of gas ionization is smaller than the one on the temperature T_0 at mean density, so we shall not consider it any further. In our numerical results we shall take $\epsilon = 1$.

4. Numerical Results.

To compute the contribution of the IGM to CMB temperature anisotropies, we take the concordance model as our fiducial cosmological model: $\Omega_\Lambda = 0.73$, $\Omega_{DM} = 0.23$, $\Omega_B = 0.04$, $h = 0.71$ and $\sigma_8 = 0.9$, in agreement with WMAP results (Spergel et al. 2003). Except when specified otherwise, we present our results for $g(\nu) = 1$. The physical parameters describing IGM thermal evolution history: the temperature T_0 at mean density, the Jeans length -fixed by T_m - and the polytropic index γ , are the free parameters of our model. When the temperature of the IGM increases (e.g., during the re-ionization of He at $z \approx 3$.) so does the Jeans length. Then, perturbations that were previously evolving are frozen or partly damped. Suppression of power on smaller scales can also happen at an early epoch by energy injection (Springel et al. 2001). Since the contribution of those scales will be erased, one would require a detailed study of the evolution of T_m with redshift to estimate the CMB temperature anisotropies. To be conservative, we shall take it equal to the largest admissible value instead of the average IGM temperature. The HeII re-ionization at $z \approx 3$ requires temperatures larger than 5×10^4 K (Schaye et al. 2000). Hui & Haiman (2003) argued that the IGM reached higher values during its thermal history. Analyzing the SDSS data, Viel & Haehnelt (2005) found that the temperature range is weakly constrained and gave an upper bound of $T_m \approx 2 \times 10^5$ K. For our numerical estimates we adopt a maximum value of $T_m = 1 \times 10^5$ K. With respect to the temperature at mean density we take an average of $T_0 = 1.4 \times 10^4$ K according to the lower values obtained by Hui & Haiman (2003). This temperature is mainly determined by the equilibrium of the photoionization due to the UV background radiation and recombination of hydrogen at mean density. This value is also within the range obtained from the analysis of the QSO absorption lines (Stocke et al. 2004). Finally, our numerical estimates depend critically on the redshift evolution of γ , that is very uncertain and strongly model dependent. Since our results show (see below) that most of the contribution to the CMB temperature anisotropy is generated in the redshift interval $z \approx 0.1 - 0.4$, we can fix γ to be the average value in that redshift interval.

Our current ideas of galaxy formation suggest that above $z = 6$ an increasing fraction of the gas is neutral and with low temperature; on those grounds, we do not expect a large contribution from earlier epochs. Therefore, all integrations were carried up to $z_f = 6$, the epoch when the re-ionization can be considered complete.

4.1. Mean Comptonization.

Eq. (11) gives the average y -parameter distortion produced by the IGM. In Fig. 2 we show the dependence of the amplitude of the average Comptonization parameter $y_{c,av}$ with

respect to the parameter γ . In the figure, σ_8 varies from 0.7 (bottom) to 1.1 (top) in units of one tenth.

4.2. Radiation Power Spectrum.

In Fig. 3a we show several spectra for different values of $\sigma_8\gamma^2$. The amplitude of the radiation power spectrum at all scales is strongly dependent on this product (see eqs. 13-16). The small wiggle at $l = 10 - 50$ is caused by using the approximated correlation function given by eq. (16) at large angular scales. In Fig. 3b, diamonds show the variation of the power spectrum maximum amplitude as a function of $\sigma_8\gamma^2$. It corresponds to a scaling $C_{l,max}^{IGM} \sim (\sigma_8\gamma^2)^{12}$. Due to this strong dependence, if σ_8 is known, even an order of magnitude estimate of the IGM contribution to temperature anisotropies will give a rather accurate measurement of the polytropic index γ . In the same Fig. 3b, asterisks show the location of the radiation power spectrum maxima and the dashed line corresponds to the best fit. Here the dependence is much weaker and, in our range of cosmological parameters, the maximum anisotropy corresponds to angular scales ranging from 5 to 10 arcmin.

4.3. Contribution of different redshift intervals.

Due to its definition, T_0 is expected to vary little with redshift, and any time dependence can be easily incorporated into the analytical expressions. On the other hand, the polytropic index γ is strongly dependent on the thermal history of the IGM. In our calculations we have assumed that T_0 and γ are strictly constant during the cosmic evolution of the IGM from re-ionization till today. Even in this simplified model not all redshifts contribute equally to CMB distortions and temperature anisotropies. In Fig. 4a we show the differential growth of the Comptonization parameter with respect to redshift $dy_{c,av}/dz$ for different γ . In the figure, the redshift intervals are $\Delta z = 0.001$. Let us remark that when γ is small, the contribution of the IGM to $y_{c,av}$ at high redshifts ($z > 0.3$) is much higher than at smaller redshifts. For large values of γ , the gas located at redshifts $z > 1$ gives approximately equal contributions and even the low-redshift gas contributes significantly. In all cases, the contribution increases close to $z = 6$ and the choice of the upper limit of integration can affect the average distortion. As far as the IGM is well described by our model out to $z_f = 6$ our results must be taken as lower limits. For comparison, we also show the contribution of the different redshift intervals to the correlation function: $dC(0, z)/dz$ for $\gamma = 1.4$, normalized to unity at $z = 0$. In Fig. 4b we show the differential redshift contribution to the radiation power spectrum: $d/dz[l(l+1)C_l^{IGM}/2\pi]$, for different multipoles. There is a clear difference

with the behavior shown in Fig. 4a: at each multipole the signal comes preferentially from a narrow redshift range. Even if the maximum value decreases for increasing l , the effective width of redshift intervals dominating the contribution increases and the overall maximum in the full spectrum occurs at $l \approx 1000 - 3000$, as indicated by Fig. 3a.

In Figs. 2 and 3 we are implicitly assuming that all baryons are in the IGM (see eq. (2)). At high redshifts ($z = 2 - 4$) the entire baryon content of the universe can be accommodated within the warm ($\sim 10^4$ K) photo-ionized IGM. At low redshifts, the combined fraction of baryons in warm photo-ionized IGM together with those in the WHIM could be as large as 70-80%. As indicated in Fig. 4b the radiation power spectrum originates on a very narrow redshift range, and if during that period the fraction f of baryons in the IGM is kept constant at, say, 70%, the amplitude of the power spectra, that scales like f^2 , would be reduced by a factor 2. The effect would be very small for the y -parameter since first $y_{c,av}$ scales linearly with f , and second the gas at higher redshifts, where $f \approx 1$, also contributes. Considering the strong dependence of C_l^{IGM} with γ and σ_8 , the effect of this uncertainty in the upper limit derived above is not significant.

4.4. Contribution of Different Scales.

If the main drawback of analytical treatments is to be based on simplifying assumptions and to require scaling relations derived from observations, current numerical simulations lack spatial resolution in large enough volumes to resolve the complex gas dynamics (Bond et al. 2005). Our results, detailed above, seemingly contradict those of numerical simulations carried out until present. For example, White, Hernquist & Springel (2002) and da Silva et al. (2001) analyzed whether the majority of the contribution to the TSZ angular power spectrum came from diffuse gas or gas within haloes. Fig. 5 is useful to understand the different outcome between our analytical estimates and the results obtained using cosmological hydro-simulations. In the figure, we plot the contribution of the different scales to the radiation power spectrum. We particularize for $l \approx 2000$ that in all models is close to the largest amplitude of the radiation power spectrum C_l . In the upper two curves we integrate eq. (14) from $k = 0$ to k_{max} , expressed in units of the inverse Jeans length $1/x_b$. The solid line corresponds to $\gamma = 1.4, T_m = 1 \times 10^5$ K and the dashed line to $\gamma = 1.3$ at the same T_m . Let us remark that even for a fixed T_m the Jeans length varies with the polytropic index γ . The lower two curves show the differential contribution to C_{2000} of different scale intervals. We integrate eq. (14) in bins of width $\Delta k = 0.2/x_b$. Lines correspond to the same parameters as before. The amplitudes are different depending on model parameters, but both curves have very similar shape. The plot clearly shows that the main contribution to C_l comes from

scales in the range $kx_b \simeq (0.5 - 3)$. About 80 to 90% of the total power comes from scales in that range, the exact figure depending on model parameters.

In a model with $\gamma = 1.4$, $T_m = 1 \times 10^5 \text{K}$, the Jeans length is $x_b = 470h^{-1} \text{kpc}$. High-resolution hydrodynamical simulations with ARM techniques are extremely good in dealing with the gas behavior within high density regions since the refinement is governed by the local density. For example, Refregier & Teyssier (2002) studied the evolution of DM and gas with resolutions of $96h^{-1} \text{kpc}$ at $z \sim 5$ to $12h^{-1} \text{kpc}$ at $z = 0$ in the densest regions using an adaptive mesh refinement algorithm. But their resolution was much smaller in low density regions, where most of the baryons reside. SPH do not yet account for contributions that comes from scales $k \geq 2/x_b$ or are just on the edge of the necessary resolution. A SPH code evolving $2 \times (216)^3$ particles in a box of $100h^{-1} \text{Mpc}$ and cell size of $370h^{-1} \text{kpc}$ (i.e. White et al. 2002) could reach enough spatial resolution to follow the gas dynamics on scales close to the Jeans length, this is not the case. Spatial resolution is not cell size but the minimum scale below which the code is not able to solve the evolution equations. Particle mesh codes include a force cut-off at small distances resulting on a damping of the power spectrum up to 8 times the cell size (Refregier & Teyssier 2002). Even if White et al. (2002) had a effective resolution much larger than their cell size and could not account for the effect of gas on scales close to the Jeans length, they did find a 25% contribution coming from regions with density contrast ≤ 100 at $l = 2000$. This contribution was less than 2% at $l = 6000$ much as it could be expected if the signal was due to diffuse gas. As Fig. 3a shows, between those multipoles the power decreases by a factor 3 – 10, depending on the IGM temperature and polytropic index.

4.5. Contribution of different density contrasts and Jeans length.

Analytic calculations based on the halo model correctly account for the SZ contribution of gas in clusters of galaxies and collapsed objects. On the contrary, a log-normal description of baryons in the IGM is only valid for a limited range of over-densities. In the redshift interval $[0.1, 0.4]$, where most of the temperature anisotropy is generated, the fraction of matter with $\xi > 100$ is less than 0.3% (see Fig. 1). Since the log-normal PDF weights heavily the high density regions, even this fraction could have a large contribution. Observationally, it has been established that the model describes rather well Ly- α clouds with over-densities $\xi \leq 50$ by $z = 3$. Recent analysis, see e.g., Tatekawa (2005), Kayo, Taraya & Syto (2001), have shown that as a result of cosmic evolution, the density distribution becomes increasingly better described by a log-normal PDF at $z \rightarrow 0$. In particular, it was shown by Kayo et al. (2001) that it accurately describes the density distribution even in the non-linear regime up

to $\xi < 100$. Baryons at much higher densities ($\xi > 500$) will cluster in halos and experience different astrophysical processes such as shock heating, radiative effects, star formation, energy injection through supernovae explosions, etc., occurring on galaxy and cluster scales. Those baryons can not be described as a gas with uniform temperature and polytropic equation of state. As remarked in Sec. 3, averages in eqs. (9) and (13) have been carried out excluding regions with over-densities $\xi > 100$. In Fig. 6a we examine how the maximum amplitude of the radiation power spectrum $C_{l,max}$ scales with ξ_{max} for two different values of T_m . The scaling is rather weak compared to the dependence on the polytropic index γ .

The Jeans length measures the minimum scale that is gravitationally unstable. It varies with redshift as different physical processes heat and cool the gas. Then, the evolution of scales close to the Jeans length becomes rather complex. We simplify their treatment assuming T_m to be fixed and equal to its maximum value throughout its thermal evolution. Since the baryon power spectrum in eq. (3) is damped on scales smaller than the Jeans length, this assumption reduces the contribution of those intermediate scales. In Fig. 6b we plot the dependence of the maximum amplitude of $C_{l,max}$ with T_m . As expected, larger T_m lead to a smaller contribution since a smaller number of scales is included. To summarize, the scaling behavior represented in Figs. 3b and 6 is

$$C_{l,max} \sim \sigma_8^{12} \gamma^{24} T_m^{-6} \xi_{max}^{1.2} \quad (18)$$

For comparison, $C_l^{clusters} \sim \sigma_8^6$ obtained by Komatsu & Kitayama (1999) from analytical estimates. Small variations on γ can produce a strong change in the amplitude of the radiation power spectrum. Even if T_m is only known up to an order of magnitude and our model can only be applied up to over-densities $\xi \leq 20$, we could still obtain strong constraints on γ from observations of CMB temperature anisotropies.

4.6. IGM contribution to CBI scales.

In Fig. 7 we compare the CMB temperature anisotropy power spectrum of cosmological origin (solid line) with TSZ contribution of clusters of galaxies (dotted line) and the IGM (dashed line) with $\gamma = 1.4, T_m = 10^5 K$ and $\gamma = 1.27, T_m = 5 \times 10^4$. We adopted $g(32GHz) = -1.96$ to rescale the TSZ power spectra to the operating frequency of the Cosmic Background Imager (CBI) experiment (Readhead et al., 2004). CBI showed an excess over the cosmological radiation power spectrum at $l > 2000$. The result and its 1σ error box is included in the figure. Depending on model parameters, TSZ cluster and IGM components could have similar or very different amplitudes and shapes. Sadeh & Rephaeli (2004) have demonstrated that the radiation power spectrum generated by clusters depends

on the assumed mass-temperature relation and gas evolution. The cluster power spectrum represented in Fig. 7 has been generated using an analytical model that does not peak at $l = 2000$. Bond et al. (2005) found that to explain the CBI excess with the anisotropy generated by clusters requires $\sigma_8 = 1.0$ or larger. Taking into account the contribution of the IGM, it can be seen in Fig. 7 that if $\sigma_8 = 0.9$ and T_m and γ vary within the intervals $5 \times 10^4 \leq T_m \leq 10^5 K$ and $1.27 \leq \gamma \leq 1.4$, the combined power spectrum CMB+SZ cluster+IGM is fully consistent with the CBI observations. Turning the argument around, if the CBI data is assumed to be an upper limit to the total anisotropy on scales $l > 2000$, then $\gamma > 1.5$ is ruled out at the 2σ level. Since the contribution to those scales comes mostly from $z = 0.1 - 0.4$ (see Fig. 4b), this upper limit applies to the gas at that redshift.

5. Discussion.

In this article we have shown that ionized gas, in the deep potential wells of clusters of galaxies and in the IGM, have a significative effect on the CMB, generating both temperature anisotropies and spectral distortions. While the latter is proportional to the electron pressure along the line of sight, the former depends on the clustering properties of the hot gas (Hernández-Monteagudo et al. 2000). The high amplitude of the radiation power spectrum, similar in magnitude to the contribution of clusters, is due to the non-linear evolution and high degree of clustering of the baryonic matter at low redshift. It is the lognormal distribution of the ionized gas that drives the strong dependence of the amplitude of the radiation power spectrum with γ and σ_8 . This extra component can make compatible the CBI measured power excess at $l \sim 2000$ with $\sigma_8 = 0.9$. At all redshifts, the largest contribution comes from scales around the baryon Jeans length. In cosmological simulations set to compute the TSZ contribution to the Cosmic Microwave Background temperature anisotropies, this scale is not well resolved, what explains why this contribution has not yet been identified in numerical simulations.

The log-normal model is remarkable for predicting a strong dependence of the radiation power spectrum with two parameters: $C_{l,max} \sim (\gamma^2 \sigma_8)^{12}$. Even if the range of scales, densities and redshifts to which the model can be applied is rather uncertain, those parameters produce minimal variations in shape of the radiation power spectrum and the variations in the amplitude are much smaller than that of γ and σ_8 . Remarkably, the anisotropy due to the IGM is generated in a narrow redshift interval. Assuming $\sigma_8 = 0.9$, one can obtain a firm upper limit of $\gamma \leq 1.5$ at the 2σ confidence level in the redshift range [0.1-0.4]. As different redshift intervals dominate the anisotropy at different angular scales, measurements of the power spectrum at different l will allow to determine the polytropic index γ and the state of

the ionized gas at different redshifts.

By hypothesis, the gas obeys a polytropic equation of state. This cannot account for the effect of the shock heated gas of the WHIM leading to high temperatures ($T \approx 10^6 - 10^7 K$). Thus, this baryon component might provide an extra TSZ contribution at redshifts close to zero. To distinguish the IGM TSZ effect from the one coming from clusters of galaxies, it is necessary to use their different statistical properties. Since the TSZ effect is independent of redshift, the cluster signal will correlate with cluster positions on the sky. Cross-correlation of cluster catalogs with CMB maps opens the possibility of determining the cluster contribution and to separate the IGM component. Hernández-Monteagudo, Génova-Santos & Atrio-Barandela (2004) and Afshordi, Lin & Sanderson (2005) have recently carried out such an analysis using WMAP data. They found strong evidence (at the 5 and 8σ levels, respectively) of a TSZ contribution to the radiation power spectrum due to clusters but the data was not sensitive enough to yield the radiation power spectrum. The PLANCK satellite, with its large frequency coverage, will be well suited for measuring the TSZ power spectrum. It is worth to explore correlation techniques that will permit to separate the cluster from the IGM component. Measurements of the IGM power spectrum at different multipoles will provide a measurement of the state of the gas (temperature and polytropic index) at different redshifts.

JPM thanks the KITP for financial support. This research was supported in part by the National Science Foundation under Grant No. PHY99-0794. F.A.B. acknowledges financial support from the Spanish Ministerio de Educación y Ciencia (projects BFM2000-1322 and AYA2000-2465-E) and from the Junta de Castilla y León (projects SA002/03 and SA010C05).

REFERENCES

- Afshordi, N., Lin, Y.T., Sanderson, A.J.R. 2005, ApJ, 629, 1
- Atrio-Barandela, F., Mücke, J. 1999, ApJ, 515, 465
- Bi, H., Davidsen, A.F. 1997, ApJ 479, 523
- Bond et al. 2005, ApJ, 626, 12
- Cen, R., Ostriker, J.P. 1999, ApJ, 519, L109
- Choudhury, T.R., Padmanabhan, T., Srianad, R. 2001, MNRAS, 322, 561
- Coles, P., Jones, B. 1991, MNRAS 248, 1

- da Silva et al. 2001, ApJ, 561, L15
- Dave, R., Hernquist, L., Katz, N., Weinberg, D.H. 1999, ApJ, 511, 521
- Dave, R., et al. 2001, ApJ, 552, 473
- Fang, L.Z., Bi, H., Xiang, S., Börner, G. 1993, ApJ, 413, 477
- Hernández-Monteagudo, C., Atrio-Barandela, F. & Mückel, J. 2000, ApJ, 528, L69
- Hernández-Monteagudo, C., Genova-Santos, R., Atrio-Barandela, F., 2004, ApJ, 613, L89
- Komatsu E., Kitayama, T. 1999, ApJ, 526, L1
- Hui, L. & Haiman, Z. 2003, ApJ 596, 9
- Kayo I., Taraya A., Suto Y. 2001, ApJ 561, 22
- Molnar, S.M., Birkinshaw, M. 2000, ApJ, 537, 542
- Rauch, M., et al. 1997, ApJ, 489, 7
- Rauch, M. 1998, ARA&A, 36, 267
- Readhead, A. C. S. et al. 2004, ApJ 609, 498
- Refregier, A., Komatsu, E., Spergel, D. & Pen, U.L. 2000, Phys. Rev. D61, 123001
- Refregier, A. & Teyssier 2002, Phys. Rev. D66, 043002
- Sadeh, S., Rephaeli, Y. 2004, New Astron, 9, 373
- Schaye, J. 2000, MNARS, 318, 817
- Schaye, J. 2001, ApJ, 559, 507
- Spergel, D.N. et al. 2003, ApJSS, 148, 175
- Springel, V., White, M. & Hernquist, L. 2001, ApJ 549, 681
- Stocke, J.T., Shull, J.M., Penton, S.V. 2004, astro-ph/0407352
- Sunyaev, R.A. & Zel'dovich, Ya. B. 1972, Comments Astrophys. Space Phys., 4, 173
- Sunyaev, R.A. & Zel'dovich, Ya. B. 1980, MNRAS, 190, 413
- Tatekawa, T. 2005, JCAP 4, 18

White, M., Hernquist, L. & Springel, V. 2002, ApJ 579, 16

Zhang, P.J., Pen, U.-L., Wang, B. 2002, ApJ, 577, 555

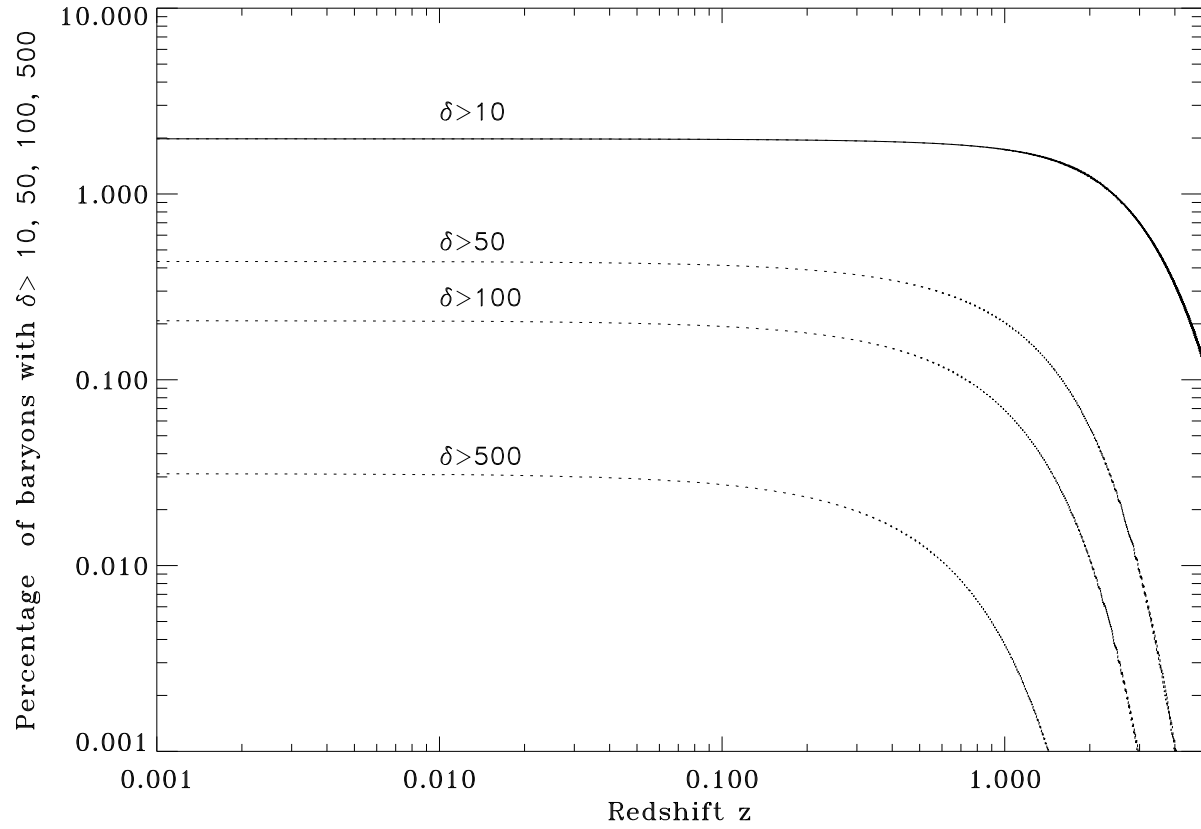


Fig. 1.— Fraction of baryons that reside in regions of density contrasts $\xi > \delta_{max} = 10, 50, 100$ and 500 as a function of redshift.

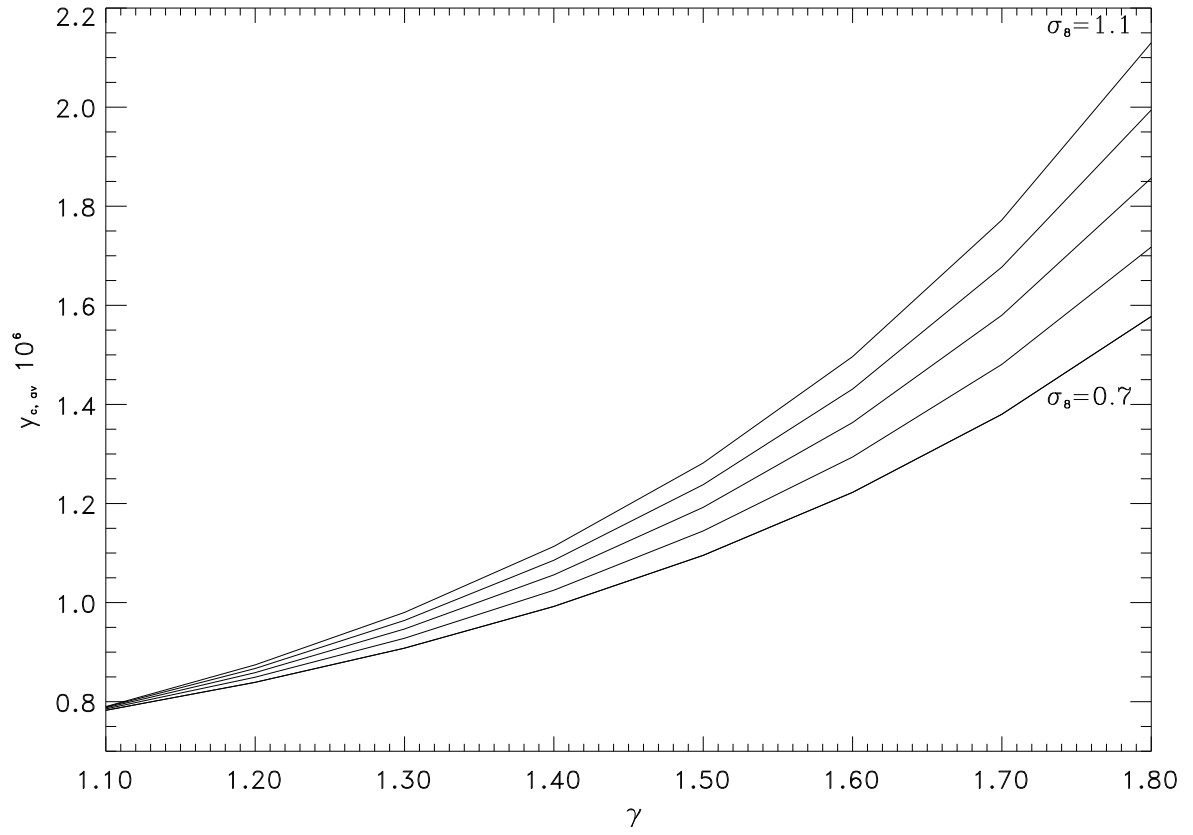


Fig. 2.— Mean Comptonization parameter $y_{c,av}$ as a function of the polytropic index γ . Curves correspond to different value of σ_8 . From top to bottom, curves decrease in units of one tenth.

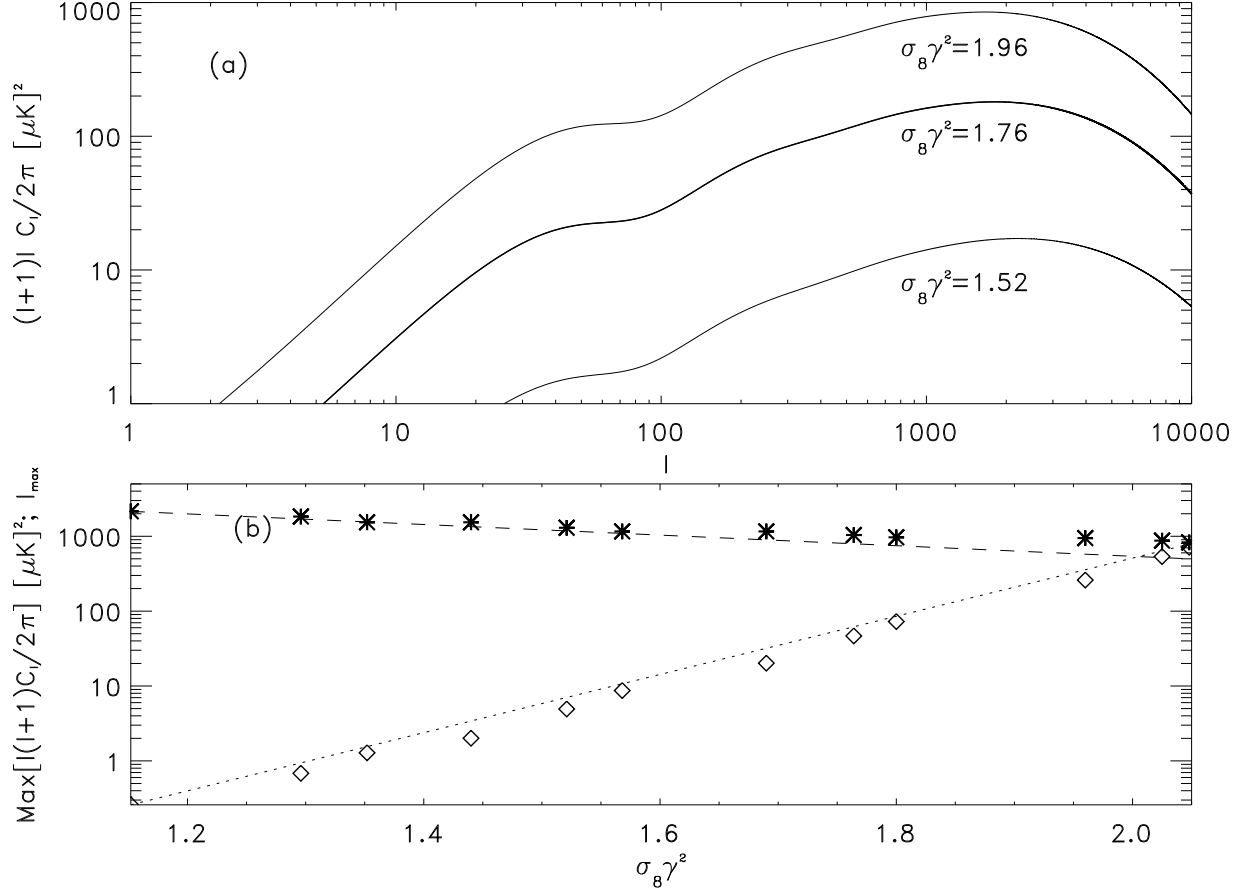


Fig. 3.— (a) CMB radiation power spectrum. The middle curve corresponds to $\gamma = 1.4$, $\sigma_8 = 0.9$. (b) Best fit to the amplitude (dotted line) and location (dashed line) of the radiation power spectrum maxima as a function of combined gas and cosmological parameters ($\sigma_8 \gamma^2$). Asterisk and diamonds correspond to the models actually computed. The y-axis gives the maximum value in (μK^2) -diamonds- and the multipole l_{max} corresponding to the maxima -asterisks-.

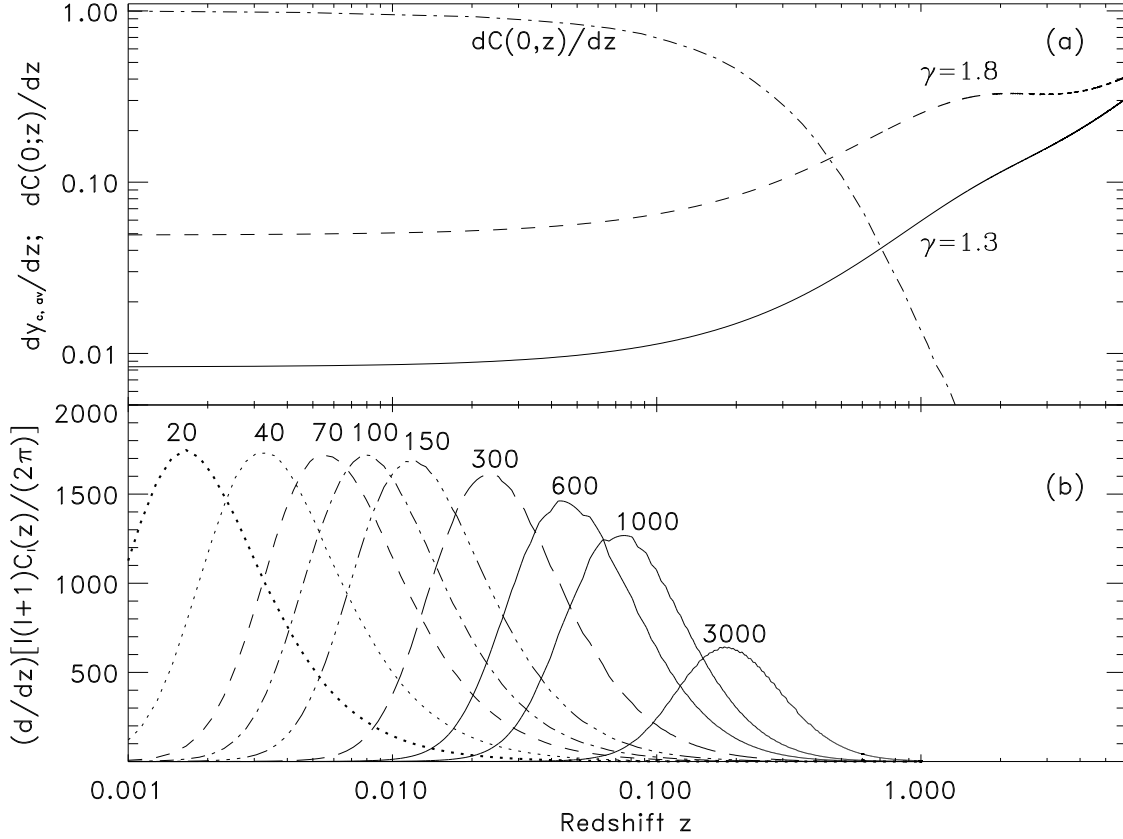


Fig. 4.— (a) Contribution of the IGM at different redshift intervals, to the Comptonization parameter in redshift bins of $\Delta z = 0.001$, for different parameters. The dash-dotted line shows the time dependence of $dC(0; z)/dz$ (normalized to unity at $z = 0$). (b) Contribution to the radiation power spectrum of redshift bins of width $\Delta z = 0.001$ as a function of redshift $d[l(l + 1)C_l]/dz$ for fixed multipoles l ($\gamma = 1.4$, $\sigma_8 = 0.9$).

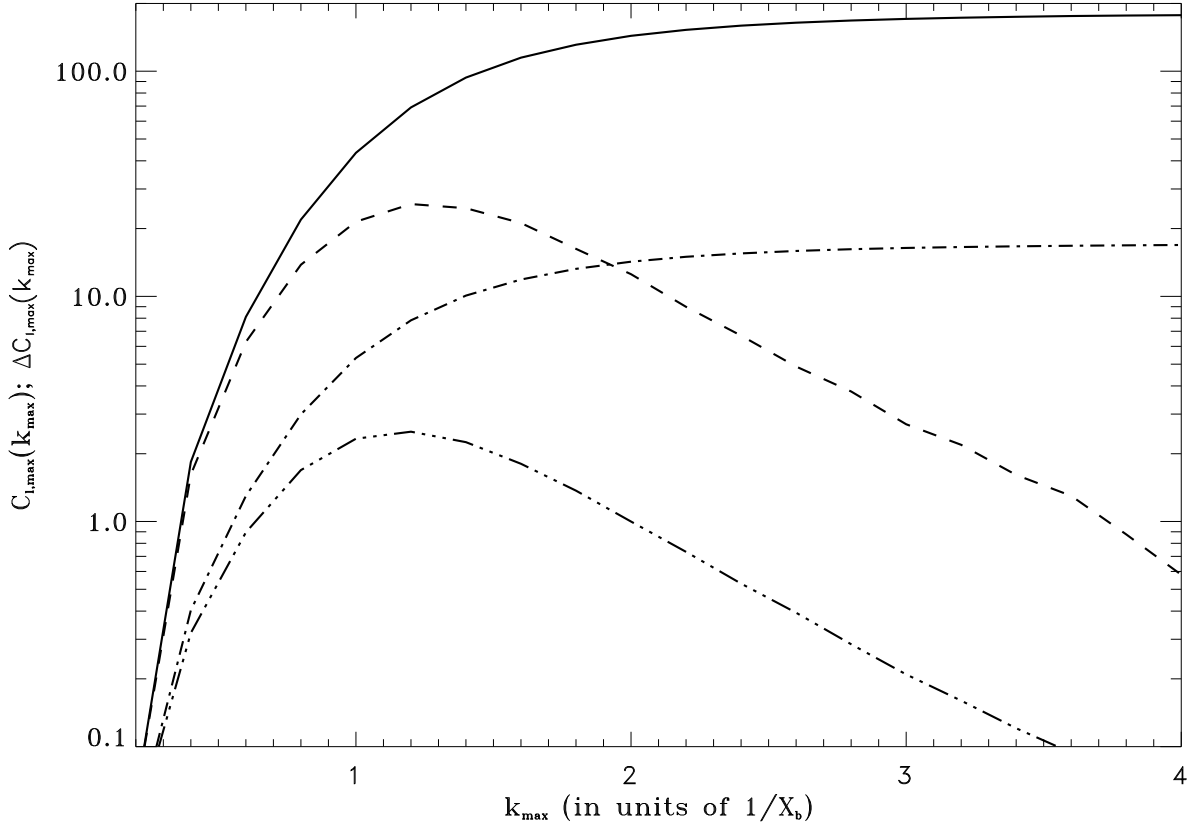


Fig. 5.— Upper curves: contribution to $C_{l,max}$ of all scales $k \leq k_{max}$ (k_{max} in units of x_b), i.e., when the integral over k in eq. (14) is restricted to that interval. Solid line corresponds to $\gamma = 1.4, T_m = 10^5 K$, dash-dotted line to $\gamma = 1.3 K$. Lower curves (dashed and dash-triple dotted) : contribution per bins of width $\Delta k = 0.2/x_b$ to $C_{l,max}$.

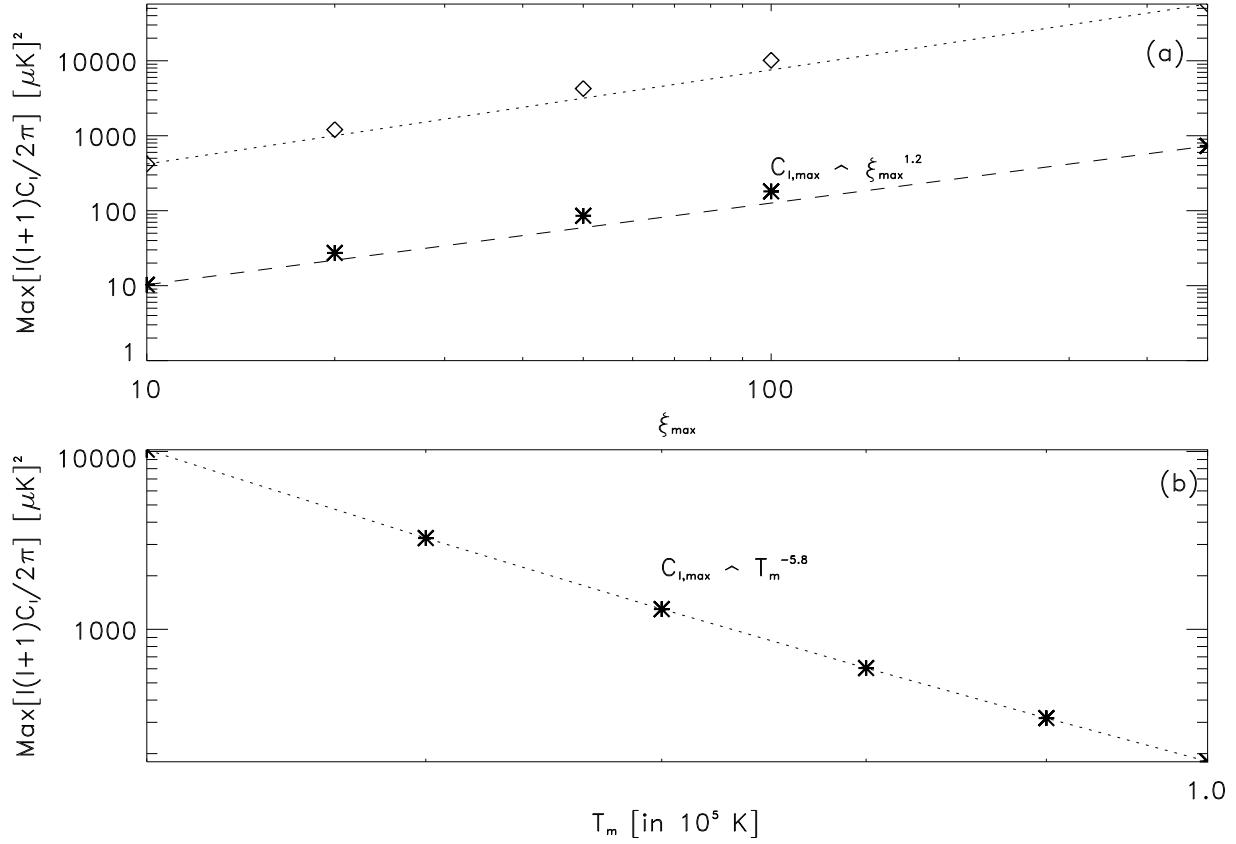


Fig. 6.— Scaling of the maximum amplitude of the radiation power spectrum $C_{l,\text{max}}$ with (a) ξ_{max} and (b) T_m . All models have $\sigma_8 = 0.9$, $\gamma = 1.4$. In (a) dotted line corresponds to $T_m = 5 \times 10^4$ K and dashed line to $T_m = 1 \times 10^5$ K. In (b) $\xi_{\text{max}} = 100$.

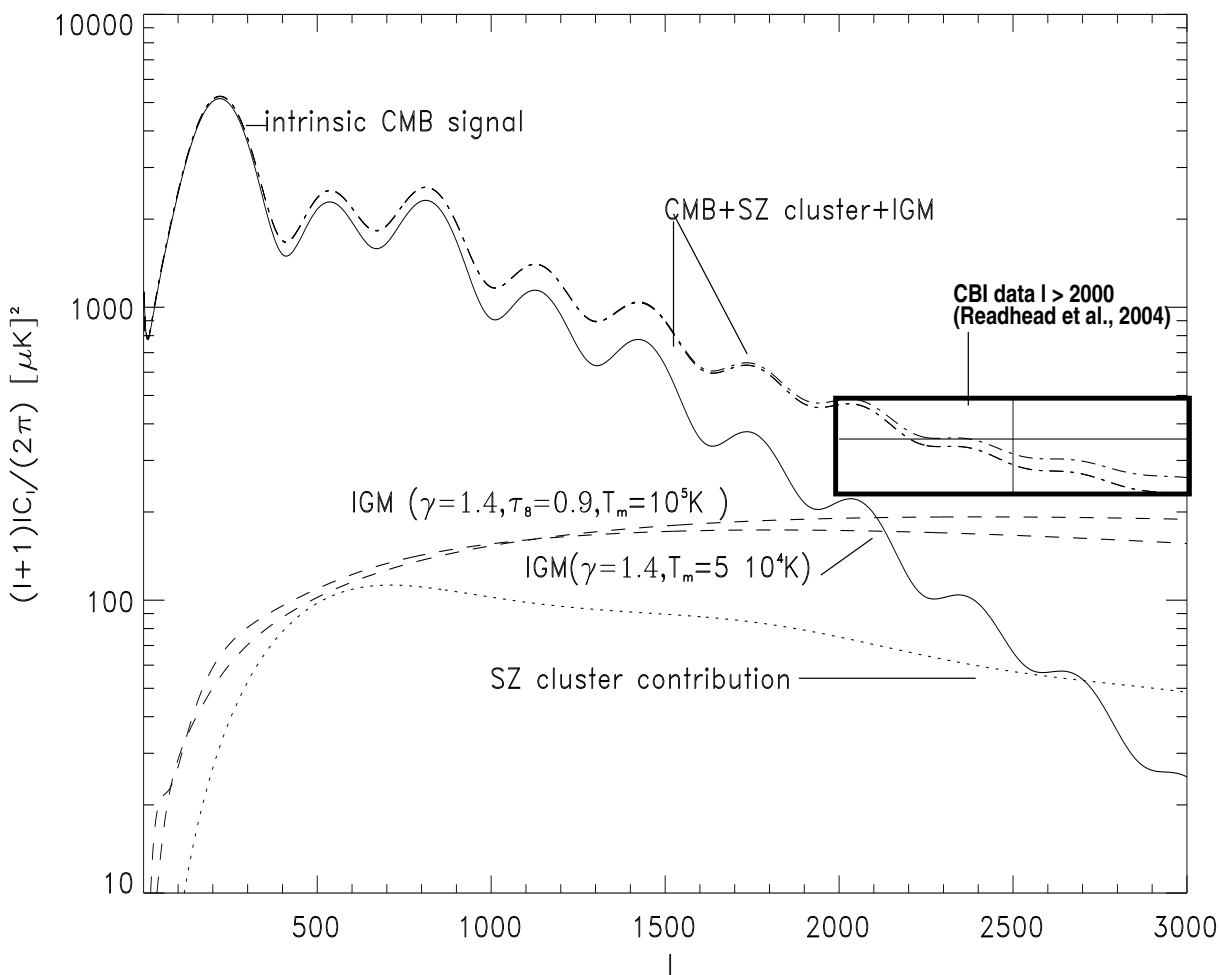


Fig. 7.— TSZ radiation power spectrum component from clusters (dotted line) and IGM (dashed) for two different polytropic indices, intrinsic CMB temperature anisotropies (solid) and the sum of the three components (dot-dashed). The TSZ power spectrum has been rescaled to 32 GHz. The box gives the CBI data at the scales of interest.